Inorganic Chemistry

Article

pubs.acs.org/IC

β-Nitro Derivatives of Iron Corrolates

Sara Nardis,[†] Manuela Stefanelli,[†] Pruthviraj Mohite,[†] Giuseppe Pomarico,[†] Luca Tortora,[†] Machima Manowong,[‡] Ping Chen,[‡] Karl M. Kadish,[‡,*] Frank R. Fronczek,[§] Gregory T. McCandless,[§] Kevin M. Smith,[§,*] and Roberto Paolesse[†,*]

[†]Dipartimento di Scienze e Tecnologie Chimiche, Università di Roma Tor Vergata, via della Ricerca Scientifica, 1, 00133 Rome, Italy,

[‡]Department of Chemistry, University of Houston, Houston, Texas, 77204-5003, United States

[§]Department of Chemistry, Louisiana State University, Baton Rouge, Louisiana 70803, United States

Supporting Information

ABSTRACT: Two different methods for the regioselective nitration of different *meso*-triarylcorroles leading to the corresponding β-substituted nitrocorrole iron complexes have been developed. A two-step procedure affords three Fe(III) nitrosyl products—the unsubstituted corrole, the 3-nitrocorrole, and the 3,17-dinitrocorrole. In contrast, a one-pot synthetic approach drives the reaction almost exclusively to formation of the iron nitrosyl 3,17-dinitrocorrole. Electron-releasing substituents on the *meso*-aryl groups of the triarylcorroles induce higher yields and longer reaction times than what is observed for the synthesis of similar triarylcorroles with electron-withdrawing functionalities, and these results can be confidently attributed to the facile formation and stabilization of an intermediate iron corrole π-cation radical. Electron-withdrawing substituents on the *meso*-aryl groups of triarylcorrole also seem to labilize the axial nitrosyl group which, in the case of the pentafluorophenylcorrole derivative, results in the direct formation of a disubstituted iron μ-oxo dimer complex. The influence of *meso*-aryl substituents on the progress and products of the nitration reaction was investigated. In addition, to elucidate the most important factors which influence the redox reactivity of these different iron nitrosyl complexes, selected compounds were examined by cyclic voltammetry and thin-layer UV−visible or FTIR spectroelectrochemistry in CH_2Cl_2.

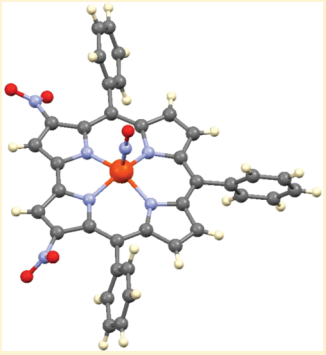

INTRODUCTION

Among the earliest examples of synthetic porphyrinoid macrocycles to be compared to the parent porphyrins are the corroles (Scheme 1), which were reported for the first time in the 1960s by Johnson and Kay.[1] Although these macrocycles have been studied for many decades, it is only recently that several research groups have focused their attention on these compounds,[2,3] taking advantage of the significant advances achieved with respect to new synthetic protocols leading to triarylcorroles in high yield.[4,7]

One reason for this recent interest in corroles and metallocorroles is the peculiar behavior exhibited by these macrocycles,[4−6,8] which are endowed with an interesting reactivity profile due in large part to the lower symmetry of the contracted ring which, in the case of peripheral functionalization, may lead to unexpected products[4] and unexpected regioselectivity.[4,9] In addition to this synthetic aspect, there is also the corrole's intriguing coordination chemistry, characterized by the so-called "non-innocent" behavior of the macrocyclic ligand.[10,11]

Many features particular to the corroles can be largely attributed to the structure of the macrocycle, which is a trianionic ligand, having three inner core amine protons within a contracted tetrapyrrolic ring. These characteristics lead, on one hand, to a stabilization of the central metal ion in a formally higher oxidation state than for similar porphyrins and, on the other hand, to a facile oxidation of the macrocyclic ring, giving π-cation radical species that exhibits an intramolecular ligand-to-metal charge transfer band. This feature sometimes makes it difficult to elucidate the electronic structure of metallocorroles, but at the same time it opens up interesting opportunities for both the functionalization and the further exploitation of metallocorrole derivatives.

In this regard, we have recently shown that a nitration reaction carried out on an iron triarylcorrolate[12] confirmed the noninnocence[10,11] of the macrocyclic ligand in these complexes. With this and previous results in mind, we decided to extend our initial study of the nitration reaction to other iron triarylcorrolates in order to investigate the scope of the synthetic method. Since our hypothesis was based on involvement of a corrole π-cation radical substrate[11−13] which would undergo nucleophilic attack by the nitrite ion, we wished to evaluate how different *meso*-aryl substituents would effect formation of the reactive species and also the yield of the reaction. For this reason, both electron-withdrawing and electron-donating groups were introduced onto the substrates of the nitration reaction (Scheme 1).

A second important aspect of this project was to understand how nitro substituents introduced at the β-pyrrole and/or *meso*-

Received: February 2, 2012
Published: March 6, 2012

 © 2012 American Chemical Society dx.doi.org/10.1021/ic3002459 | *Inorg. Chem.* 2012, 51, 3910−3920

Scheme 1. Nitration of Triarylcorroles

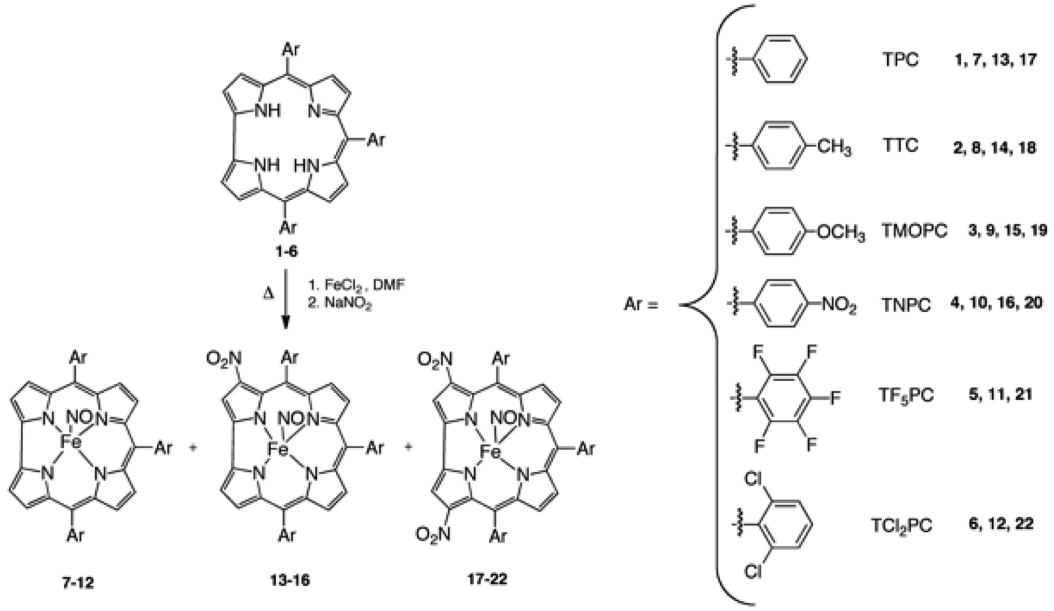

Table 1. Yields of Products

H_3TArC	method	time (min)	TArCFe-NO (yield %)	(NO_2)TArCFeNO (yield %)	$(NO_2)_2$TArCFeNO (yield %)	$[(NO_2)_2TArCFe]_2O$ (yield %)
1	A	120	10%	12%	27.8%	
	B	45		trace	27.5%	
2	A	120	9%	11%	26%	
	B	45			28%	
3	A	120	14%	17%	27%	
	B	45	–	–	36%	
4	A	75	10.7%	12%	17.2%	
	B	40			5%	–
5	A	90	5%	Mixture		9.2%
	B	90			5.8%	9%
6	A	45	trace		32.6%	
	B	25			22.6%	

phenyl positions of the macrocycle would influence both the redox potentials and the site of electron transfer in the synthethized compounds. This is examined in the present study where we report electrochemical and spectroscopic characterization of the synthesized iron nitro complexes in CH_2Cl_2.

EXPERIMENTAL SECTION

Materials. Silica gel 60 (70–230 mesh, Sigma Aldrich) or neutral alumina oxide (Grade III, Merck) were used for column chromatography. Reagents and solvents for syntheses (Aldrich, Merck or Fluka) were of the highest grade available and were used without further purification. ^{1}H NMR spectra were recorded on a Bruker AV300 (300 MHz) spectrometer. Chemical shifts are given in ppm relative to residual $CHCl_3$ (7.25 ppm). UV–vis spectra were measured on a Cary 50 spectrophotometer. Mass spectra (FAB mode) were recorded on a VGQuattro spectrometer in the positive-ion mode using *m*-nitrobenzyl alcohol (Aldrich) as a matrix.

Absolute dichloromethane (CH_2Cl_2, 99.8%, EMD Chemicals Inc.) was used for electrochemistry without further purification. Tetra-*n*-butylammonium perchlorate (TBAP), used as supporting electrolyte, was purchased from Sigma Chemical or Fluka Chemika Co., recrystallized from ethyl alcohol, and dried under vacuum at 40 °C for at least one week prior to use.

Electrochemistry. Cyclic voltammetry was carried out with an EG&G Model 173 potentiostat/galvanostat. A homemade three-electrode electrochemistry cell was used and consisted of a platinum button or glassy carbon working electrode, a platinum wire counter electrode, and a saturated calomel reference electrode (SCE). The SCE was separated from the bulk of the solution by a fritted-glass bridge of low porosity, which contained the solvent/supporting electrolyte mixture. All potentials are referenced to the SCE.

Thin-layer UV–visible spectroelectrochemical experiments were performed with a home-built thin-layer cell which has a light transparent platinum net working electrode. Potentials were applied and monitored with an EG&G PAR Model 173 potentiostat. Time-resolved UV–visible spectra were recorded with a Hewlett-Packard Model 8453 diode array spectrophotometer. High purity N_2 from Trigas was used to deoxygenate the solution and kept over the solution during each electrochemical and spectroelectrochemical experiment.

Thin-layer FTIR spectroelectrochemical measurements were obtained using a Nicolet 6700 FTIR spectrometer along with an EG&G model 173 potentiostat and a specially constructed light-transparent three-electrode cell.[14] The measured background consists of a combination of the IR spectrum of the compound, that of the supporting electrolyte, and that of the solvent saturated with N_2 (or other gases as noted). Therefore, the spectra of the reduced and oxidized complexes are displayed as difference spectra with respect to the initial compound. A negative peak corresponds to a disappearance of the reactant IR band, and a positive peak corresponds to an IR band of the electrogenerated product.

dx.doi.org/10.1021/ic3002459 | Inorg. Chem. 2012, 51, 3910–3920

Syntheses. The free-base triarylcorroles (H_3TArC) **1**–**6** were prepared according to published procedures.[4,6,15–17] The iron complexes were then prepared following two similar procedures, referred to as Method A and Method B, which differ from each other by the amount of iron chloride in the nitration reaction medium.

Method A. H_3TArC (1 mmol) and $FeCl_2$ (20 mmol) were dissolved in DMF (30 mL), and the resulting mixture was heated to reflux; water was added to precipitate the product after formation of the complex was evidenced by UV–vis spectrophotometry and TLC. The precipitate was then filtered, dissolved in CH_2Cl_2, and dried over anhydrous Na_2SO_4, and after evaporating the solvent under vacuum, the residue was used without further purification for the nitration reaction. For this purpose, the iron complex was dissolved in DMF, and $NaNO_2$ (150 mmol) was added. The progress of the reaction was monitored by TLC and UV–vis spectrophotometry, following the disappearance of the starting material. After precipitation by addition of water and filtration, the crude mixture was dissolved in CH_2Cl_2 and dried over anhydrous Na_2SO_4, and the solvent was evaporated. Purification by chromatography on a silica gel column using CH_2Cl_2 (or $CHCl_3$ for TNPC and TF_5PC) as eluant, followed by recrystallization from CH_2Cl_2/MeOH (1:2), afforded the desired compounds.

Method B. H_3TArC (1 mmol) was dissolved in DMF (30 mL); $FeCl_2$ (5 mmol) was added, and the resulting solution was refluxed for 90 min. During this period the color changed from purple to brown, indicating formation of the corresponding iron complex, which was confirmed by UV–vis spectrophotometry. $NaNO_2$ (150 mmol) was then added to the hot solution and the progress of the reaction monitored by TLC and UV–vis spectrophotometry. After allowing the reaction to proceed for 45 to 120 min (the exact time depending on the specific starting corrole), water was added and the precipitate was collected after filtration. The subsequent reaction workup was performed as described in Method A.

The yields of the products, for each of the two described methods, are listed in Table 1.

(TArPC)FeNO. **7**, **8**, **9**, **10**, and **11** were characterized by comparison with an authentic sample prepared according to literature methods,[18] while **12** was isolated in trace amounts and identified by comparison with literature UV–vis data.[19] Spectroscopic data for **13**, **14**, **17**, and **18** were in agreement with data reported earlier in the literature.[12]

3-NO_2-(TMOPC)FeNO ***15***. ^{1}H NMR (300 MHz, $CDCl_3$, J [Hz]): δ = 8.47 (s, 1H, β-pyrrole), 7.98 (d, 1H, J = 4.6, β-pyrrole), 7.89 (d, 1H, J = 4.5, β-pyrrole), 7.82 (d, 2H, J = 8.5, phenyl), 7.68 (m, 7H, β-pyrrole and phenyl), 7.55 (d, 1H, J = 4.9, β-pyrrole), 7.15 (m, 6H, phenyl), 4.01 (s, 3H, $-OCH_3$), 3.99 (s, 3H, $-OCH_3$) 3.97 (s, 3H, $-OCH_3$). UV–vis (CH_2Cl_2): λ_{max} (log ε) = 431 (4.8), 568 nm (4.3). MS (FAB): m/z 714 (M^+ − NO). Anal. Calcd for $C_{40}H_{28}FeN_6O_6$: C, 64.53; H, 3.79; N, 11.29. Found: C, 64.44; H, 3.84; N, 11.18.

3-NO_2-(TNPC)FeNO ***16***. ^{1}H NMR (300 MHz, $CDCl_3$, J [Hz]): δ = 8.71 (s, 1H, β-pyrrole), 8.53 (m, 6H, phenyl), 8.19 (d, 1H, J = 4.65, β-pyrrole), 8.08 (d, 2H, J = 7.74, phenyl), 8.00 (d, 1H, J =8.1, phenyl), 7.91 (m, 4H, phenyl), 7.70 (d, 1H, J = 4.8, β-pyrrole), 7.63 (d, 1H, J = 4.9, β-pyrrole), 7.55 (d, 1H, J = 4.8, β-pyrrole), 7.49 (d, 1H, J = 5, β-pyrrole). UV–vis (CH_2Cl_2): λ_{max} (log ε) = 423 (4.9), 588 nm (4.5). MS (FAB): m/z 759 (M^+ − NO). Anal. Calcd for $C_{37}H_{19}FeN_9O_9$: C, 56.29; H, 2.43; N, 15.97. Found: C, 56.18; H, 2.61; N, 16.01.

3,17-$(NO_2)_2$ -(TMOPC)FeNO ***19***. ^{1}H NMR (300 MHz, $CDCl_3$, J [Hz]): δ = 8.48 (s, 2H, β-pyrrole), 7.89 (d, 2H, J = 5, β-pyrrole), 7.70 (m, 8H, β-pyrrole and phenyl), 7.15 (m, 6H, phenyl), 4.00 (s, 3H, $-OCH_3$), 3.98 (s, 6H, $-OCH_3$). UV–vis (CH_2Cl_2): λ_{max} (log ε) = 370 (4.6), 437 (4.6), 593 nm (4.4). MS (FAB): m/z 759 (M^+ − NO). Anal. Calcd for $C_{40}H_{27}FeN_7O_8$: C, 60.85; H, 3.45; N, 12.42. Found: C, 60.78; H, 3.61; N, 12.39.

3,17-$(NO_2)_2$-(TNPC)FeNO ***20***. ^{1}H NMR (300 MHz, $CDCl_3$, J [Hz]): δ = 8.75 (s, 2H, β-pyrrole), 8.56 (m, 6H, phenyl), 7.96 (m, 6H, phenyl), 7.78 (d, 2H, J = 5.0, β-pyrrole), 7.63 (d, 2H, J = 5.0, β-pyrrole). UV–vis (CH_2Cl_2): λ_{max} (log ε) = 402 (4.9), 609 nm (4.6). MS (FAB): m/z 804 (M^+ − NO). Anal. Calcd for $C_{37}H_{18}FeN_{10}O_{11}$: C, 53.26; H, 2.17; N, 16.79. Found: C, 53.22; H, 2.21; N, 16.68.

3,17-$(NO_2)_2$-(TF_5PC)FeNO ***21***. ^{1}H NMR (300 MHz, $CDCl_3$, J [Hz]): δ = 8.98, (s, 2H, β-pyrrole), 7.86 (d, 2H, J = 4.8, β-pyrrole), 7.75 (d, 2H, J = 4.8, β-pyrrole). UV–vis CH_2Cl_2): λ_{max} = 396, 613 nm. MS (FAB): m/z 939 (M^+ − NO). Anal. Calcd for $C_{37}H_6F_{15}FeN_7O_5$: C, 45.85; H, 0.62; N, 10.12. Found: C, 45.79; H, 0.68; N, 10.15.

3,17-$(NO_2)_2$-(TCl_2PC)FeNO ***22***. ^{1}H NMR (300 MHz, $CDCl_3$, J [Hz]): δ = 8.79, (s, 2H, β-pyrrole), 7.66–7.61 (m, 11H, phenyl and β-pyrrole), 7.49 (d, 2H, J = 5.0 β-pyrrole). UV–vis (CH_2Cl_2): λ_{max} (log ε) = 393 (4.7), 620 nm (4.5). MS (FAB): m/z 876 (M^+ − NO). Anal. Calcd for $C_{37}H_{15}Cl_6FeN_7O_5$: C, 49.04; H, 1.67; N, 10.82. Found: C, 48.97; H, 1.62; N, 10.78.

[3,17-$(NO_2)_2$-(TTC)Fe]$_2O$ ***23***. ^{1}H NMR (300 MHz, $CDCl_3$, J [Hz]): δ = 7.87 (s, 2H, β-pyrrole), 7.55–7.22 (m, 12H, phenyl and β-pyrrole), 7.10 (d, 2H, J = 4.60, β-pyrrole), 6.84 (br d, 1 H, J = 6.9, phenyl), 6.61 (br d, 1H, J = 7.0 phenyl), 2.59 (s, 6H, $-CH_3$), 2.43 (s, 3H, $-CH_3$). Anal. Calcd for $C_{80}H_{54}Fe_2N_{12}O_9$: C, 66.77; H, 3.78; N, 11.68. Found: C, 66.73; H, 3.81; N, 11.62.

[3,17-$(NO_2)_2$-(TF_5PC)Fe]$_2O$ ***24***. ^{1}H NMR (300 MHz, $CDCl_3$, J [Hz]): δ = 7.95, (s, 2H, β-pyrrole), 6.96 (d, 2H, J = 4.8, β-pyrrole), 6.88 (d, 2H, J = 4.8, β-pyrrole). UV–vis CH_2Cl_2): λ_{max} (log ε) = 416 (4.8), 579 (4.6), 646 nm (4.3). MS (FAB): m/z 939 (M^+-3,17-$(NO_2)_2$-(TF_5PC)FeO). Anal. Calcd for $C_{74}H_{12}F_{30}Fe_2N_{12}O_9$: C, 46.91; H, 0.64; N, 8.87. Found: C, 46.87; H, 0.57; N, 8.93.

Crystal Data for 3,17-$(NO_2)_2$-(TPC)FeNO ***17***. Crystals were grown by slow diffusion of methanol in a concentrated dichloromethane solution. Single crystal X-ray diffraction data was collected on a Nonius KappaCCD diffractometer with a Mo Kα radiation source (λ = 0.71073 Å), graphite monochromator, and Oxford Cryosystems liquid nitrogen cryostream cooler. The structure was solved by direct methods using SIR97[20] and refined using SHELXL97.[21] All non-hydrogen atoms were refined anisotropically for the two independent Fe corroles in the unit cell, with H atoms in idealized positions with a C–H bond length of 0.95 Å. Missing symmetry was sought using the ADDSYM algorithm within the PLATON single-crystal structure validation program.[22] Crystal data: $C_{37}H_{21}FeN_7O_5$, M_r = 699.46 g mol^{-1}, triclinic, space group $P\bar{1}$, a = 10.4813 (15) Å, b = 14.3141 (15) Å, c = 21.830 (3) Å, α = 74.161 (5)°, β = 77.960 (4)°, γ = 80.100 (5)°, V = 3058.5 (6) Å^3, Z = 4, F(000) = 1432, D_x = 1.519 g cm^{-3}, μ = 0.55 mm^{-1}, T = 100 K, 35466 measured reflections, 17810 independent reflections, 9725 reflections with $I > 2\sigma(I)$, R_{int} = 0.064, θ_{max} = 30.0°, θ_{min} = 2.8°, full-matrix least-squares refinement on F^2, $R_1[F^2 > 2\sigma(F^2)]$ = 0.058, $wR_2(F^2)$ = 0.161, S = 1.03, 901 parameters, 0 restraints, w = 1/[$\sigma^2(F_o^2)$ + (0.0765P)^2], $\Delta\rho_{max}$ = 0.94 e Å^{-3}, and $\Delta\rho_{min}$ = −0.34 e Å^{-3}.

RESULTS AND DISCUSSION

In a previous communication, we reported the nitration of (TTC)FeCl in DMF by using an excess of $NaNO_2$; in particular, we observed the formation of three types of Fe(III) nitrosyl corroles using a 1:100 molar ratio of corrole vs $NaNO_2$—those with an unsubstituted macrocycle, those with one β-pyrrole NO_2 substituent, and those with two β-pyrrole NO_2 substituents (Scheme 1). Upon increasing the amount of $NaNO_2$ (1:500), the dinitro-substituted corrole became the major product of the reaction (60% yield), and the other corroles were formed in only trace amounts.

Syntheses of the desired products were achieved using a 1:150 molar ratio of (TArPC)FeNO/$NaNO_2$. We have now modified the initially reported protocol,[12] with the aim of using the free-base corrole as starting material, thus avoiding the need for purification of an intermediate iron corrole complex. Following the procedure described in Method A, we obtained all three products indicated in Scheme 1, while with Method B synthesis of the dinitrocorrole was optimized as a unique reaction product.

The reaction yields, calculated with respect to the starting free-base corrole, are comparable with those obtained from the

dx.doi.org/10.1021/ic3002459 | Inorg. Chem. 2012, 51, 3910–3920

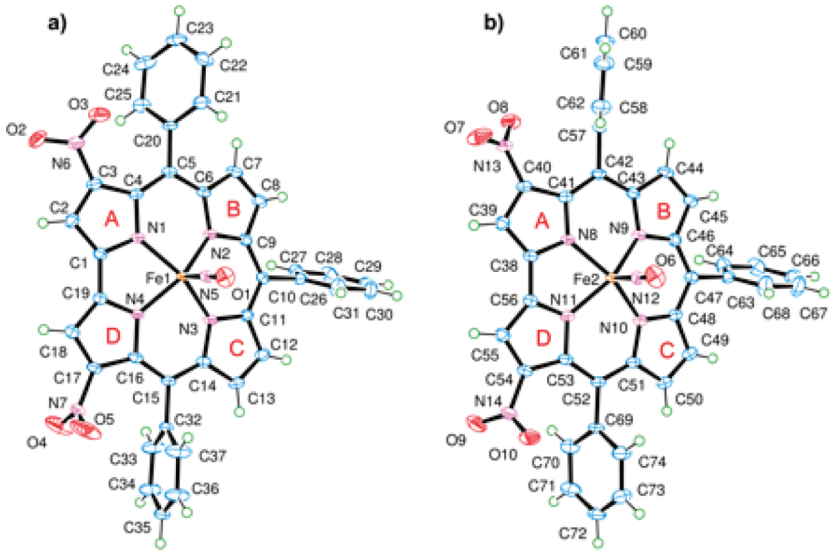

Figure 1. Two independent Fe corroles **17**, (a) Fe1 complex and (b) Fe2 complex, in the unit cell are shown in approximately the same orientation to illustrate how the respective substituents differ in orientation.

published protocol. Method A, which allowed for isolation of the three different reaction products (Scheme 1), enabled the possibility to carry out an electrochemical and spectroscopic characterization of these derivatives, thus providing additional information on the mechanism for the nitration reaction.

Although the reaction yields depend on the method used (A or B), some general trends can be observed from Table 1: electron-releasing groups present on the *meso*-phenyl rings of triarylcorroles (**2** and **3**) induced higher yields of β-nitro substituted derivatives than those obtained with corroles bearing electron-withdrawing substituents (**4** and **5**), probably due to the more facile formation of a corrole π-cation radical, which is the proposed intermediate necessary for the success of the reaction. Furthermore, for the nitration of **2** and **3** we were able to isolate all three nitrosyl complexes, while with corroles bearing electron-withdrawing substituents (**4** and **5**), we observed a more rapid disappearance of the starting material, and only in the case of **4** all the complete product series was obtained. A different behavior was observed in the case of **6**, because for this corrole the reaction always led to the isolation of a unique product, the difunctionalized corrole **22**, which was isolated in 32.6% yield in the case of Method A.

The difference in reactivity is even more evident in the case of **5**, where formation of the μ-oxo dimer **24** was observed as the major reaction product. Labilization of the nitrosyl ligand with consequent formation of the μ-oxo dimer was earlier observed in the formation of **23**[12] upon slow crystallization of **18**. The process is faster in the case of the pentafluorophenylcorrole than for the triphenylcorrole complex, and the Fe(III) nitrosyl mono- and dinitrocorroles were isolated in only trace amounts.

A plausible explanation for this behavior can lie in how the *meso* aromatic ring substituents affect the lability of the axial Fe−NO bond; this labilization can facilitate formation of a corrole π-cation radical, which then undergoes nucleophilic attack by a nitrite ion. Electron-withdrawing groups have been reported to increase the NO stretching frequencies, ν_{NO}, of the coordinated ligand,[23] evidencing a slight reduction of the bond strength between the metal center and the nitrosyl ligand and consequently supporting a labilization of the coordinated nitrosyl group.

^{1}H NMR characterization of **24** confirmed the proposed structure. The ^{1}H NMR spectrum of **21** exhibits a characteristic singlet (2H) at 8.98 ppm and two doublets at 7.86 and 7.75 ppm (two protons each); in the spectrum of the μ-oxo dimer, the two doublets at 6.88 and 6.96 ppm are identified as the proton signals of the pyrroles B and C, while the singlet at 7.94 ppm is attributed to β-pyrrolic protons at the 2- and 18-positions vicinal to the nitro groups. The overall shielding of the macrocycle signals associated with μ-oxo dimer formation is in good agreement with data reported for the unsubstituted iron complexes of **5**.[24] Similar spectral behavior is observed for **23**, which was prepared by stirring **18** in a CH_2Cl_2/CH_3OH solution.

Crystals suitable for X-ray characterization of **17** were obtained, thereby allowing an elucidation of the structure, which is illustrated in Figure 1.

There are two independent Fe corroles in the crystal structure (Figure 1), each with an almost identical corrole framework (in terms of bond lengths and angles) and angles of the linear nitrosyl group located at the axial position of the corrole, which had a 5-coordinate square pyramid environment. All of the respective Fe−$N_{nitrosyl}$ bond lengths, 1.651 (2) Å and 1.652 (2) Å; N−O bond lengths for each nitrosyl ligand, 1.165 (3) Å and 1.160 (3) Å; Fe−N—O bond angles, 178.9 (2)° and 177.9 (2)°; and the average $N_{nitrosyl}$—Fe−$N_{pyrrole}$ bond angle, 103.6°, which ranges between 102.4 (1)° and 104.5 (1)°, are comparable to other previously reported crystal structures for nitrosyl iron corrole complexes.[18,19,25,26] Similarities can also be observed with crystallographic data published for other iron−metalated complexes of triarylcorroles[12,18,19,24,26−28] in regards to the "domed conformation" and the Fe−$N_{pyrrole}$ bond length, with a minimum of 1.903 (2) Å, a maximum of 1.931 (2) Å, and an average of 1.915 Å, of this square pyramidal compound.

The planarities of the four pyrrole nitrogen atoms in the two independent molecules in the crystal structure of **17** are not quite identical (the root-mean-square deviation of least-squares planes for N1, N2, N3, N4 and N8, N9, N10, N11 are 0.0061 Å and 0.0243 Å, respectively). Out of these respective planes of the pyrrole nitrogens, the Fe atomic sites deviate toward the axial nitrosyl ligand by approximately the same distance (i.e., a deviation of 0.456 (1) Å for Fe1 and 0.444 (1) Å for Fe2). The

dx.doi.org/10.1021/ic3002459 | *Inorg. Chem.* 2012, 51, 3910−3920

characteristic tilt of the pyrrole subunits is also noted with the deviations of the pyrrolic nitrogen atoms which buckle on the same side as the axial nitrosyl ligand and are located above a fitted plane of the β-pyrrole carbons (average nitrogen atomic site deviation of 0.17 Å from the two respective least-squares planes of C2, C3, C7, C8, C12, C13, C17, C18 and C39, C40, C44, C45, C49, C50, C54, C55). Using the standard A, B, C, D labels for identification of the corrole five-membered rings (as shown in Figure 1), a range of dihedral angles between neighboring pyrrole groups, 1.5(2)−14.4(2)°, is observed in the calculations based on the refined model, with the largest dihedral angle occurring for both independent iron corroles between pyrrole A and B.

The most interesting packing relationship in the crystal structure is between the two different Fe complexes, Fe1 corrole and Fe2 corrole (shown in Figure 2), where the closest

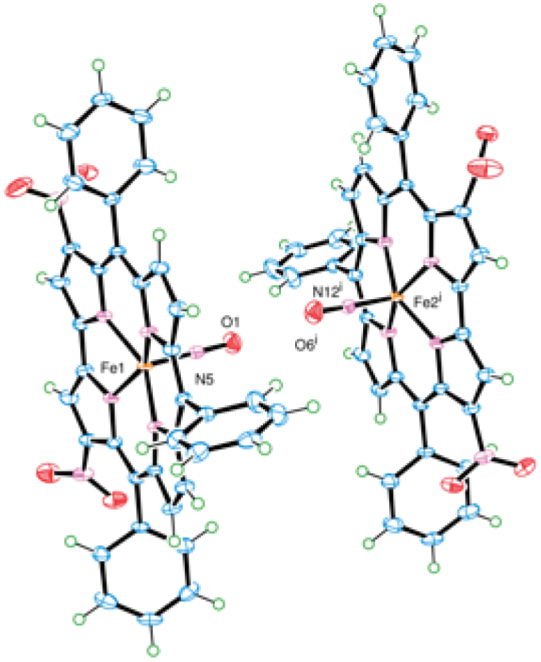

Figure 2. Packing relationship between Fe1 corrole and Fe2^{i} corrole related by the symmetry code (i) $-x + 1, -y, -z + 1$. The orientation of the axial nitrosyl ligand in each complex is pointed toward each other with a short intermolecular O1···O6^{i} distance of 2.897 (3) Å.

Fe2 corrole is located in the adjacent unit cell and related by the symmetry code (i) $-x + 1, -y, -z + 1$. The reason for this interest lies in the orientation of the axial nitrosyl ligands of each complex, which are pointed toward each other and have a short intermolecular O1···O6^{i} distance of 2.897 (3) Å without any traces of residual electron densities in between the two oxygen atomic sites. The authors are unaware of any other reported examples of axial nitrosyl ligands with such a short O···O distance. For more information on this contact and other packing relationships refer to the Supporting Information.

Method B was shown to be more selective from a preparative point of view, leading to the isolation of a 3,17-dinitrated compound as the major product. In no case did we observe formation of the unsubstituted nitrosyl iron corrole complex, while only trace amounts of the mononitro derivative **13** was obtained. In particular, for **1** and **3**, along with the 3,17-dinitrocorrole major product, it was possible to collect traces of the 2,17-dinitro compound, together with small amounts of a compound compatible with an asymmetrical trinitrocorrole as characterized by the presence of three singlets (1H each) in the ^{1}H NMR spectrum; however, the small amount of product obtained did not allow us to completely characterize this product.

It is interesting to note that a similar one-pot method has already been published for the preparation of an iron nitrosyl octaalkylcorrole;[25] the authors reported the formation of this complex by adding the required amount of sodium nitrite to a refluxing pyridine/MeOH mixture of the corrole and iron chloride. In this case, the failure to observe formation of β-nitro derivatives can be attributed to the presence of pyridine as the reaction solvent; pyridine leads to the formation of a Fe(III)−bispyridinium complex having no π-cation radical character and thereby making the complex unreactive toward nucleophilic attack and further avoiding the β-functionalization observed when DMF is used as the solvent.

Electrochemistry and Spectroelectrochemistry. Six iron corroles were chosen as representative to electrochemically investigate the effect of nitration on the overall oxidation/reduction mechanisms and site of each electron transfer. The addition of a NO_2 group at one or two β-pyrrole positions of the corrole macrocycle or on the three *meso*-phenyl groups of the triarylcorrole would be expected to shift all redox potentials toward more positive values (easier reductions and harder oxidations),[29,30] but it was not clear what would be the magnitude of the potential shift for each added electron-withdrawing NO_2 group in the case of the iron nitrosyl derivatives, nor was it clear how the addition of multiple NO_2 groups to a given corrole might effect the site of electron transfer which could occur at the central metal ion, at the conjugated π-ring system of the macrocycle, and/or at the $C_6H_4NO_2$ groups of the triarylcorrole in the case of compounds **10**, **16**, and **20**.

In order to elucidate these points, two series of corroles were selected for electrochemical and spectroelectrochemical characterization in the nonbonding solvent CH_2Cl_2. The first, labeled as Group A in Chart 1, is comprised of compounds **9**, **15**, and **19** and represents triarylcorroles having a *para*-methoxyphenyl substituent at the three *meso*-positions of the corrole and zero, one, and two NO_2 groups at the β-pyrrole position of the macrocycle; the second group of corroles which were electrochemically characterized is labeled as Group B in Chart 1 and possesses three (**10**), four (**16**), or five electron-withdrawing NO_2 (**20**) substituents, three on the *meso*-phenyl groups of the triarylcorrole and 0, 1, or 2 at the β-pyrrole positions of the macrocycle. Thus, the six compounds in Chart 1 have 0, 1, 2, 3, 4, or 5 NO_2 substituents, respectively.

Cyclic voltammograms for five of the six corroles in Chart 1 are shown in Figures 3 and 4, and a summary of measured half-wave and peak potentials is given in Table 2. The reductions and oxidations of compounds **9**, **15**, and **19** are both illustrated in Figure 3, while only the reductions are shown for the two Group B compounds in Figure 4.

As seen from the cyclic voltammograms and table of potentials, the addition of one or two nitro substituents to the β-pyrrole positions of the macrocycle leads to similar positive shifts in $E_{1/2}$ for the first metal centered reduction and the first oxidation. For example, the $Fe^{III/II}$ transition of $(NO_2)_x$(TMOPC)FeNO is located at $E_{1/2}$ = −0.35 V for compound **9** (x = 0), while **15** (x = 1) is reduced at at $E_{1/2}$ = −0.16 V and **19** (x = 2) at $E_{1/2}$ = +0.04 V. A plot of $E_{1/2}$ vs the number of NO_2 groups on the macrocycle is linear with a slope

dx.doi.org/10.1021/ic3002459 | *Inorg. Chem.* 2012, 51, 3910−3920

Chart 1. Structures of the Electrochemically Investigated Compounds

Group A: $(NO_2)x$(TMOPC)FeNO series (x = 0, 1, 2)

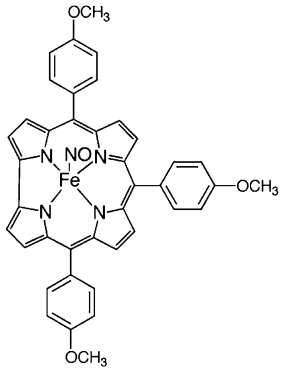

9

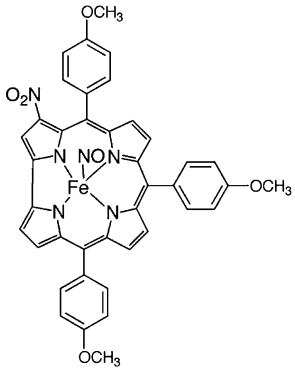

15

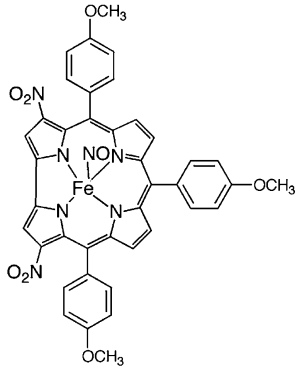

19

Group B: $(NO_2)x$(TNPC)FeNO series (x = 0, 1, 2)

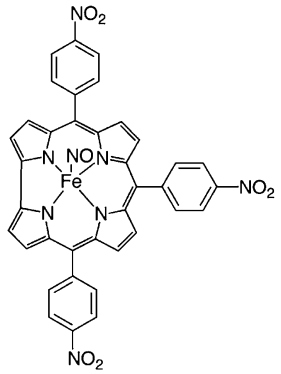

10

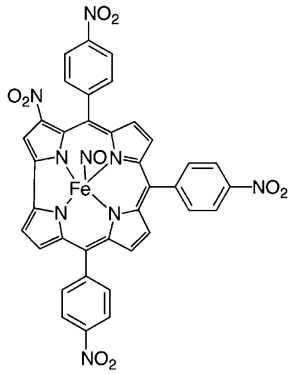

16

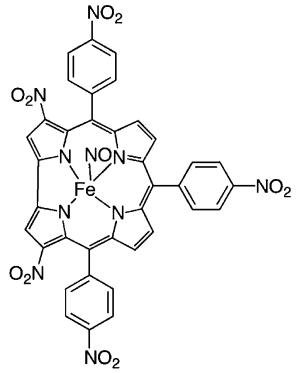

20

of 0.02 V and a correlation coefficient of 0.996. A linear relationship between $E_{1/2}$ and the number of NO_2 groups on the macrocycle is also seen for the metal-centered reductions of $(NO_2)_x$(TNPC)FeNO, and exactly the same magnitude of shift in $E_{1/2}$ with added NO_2 groups (200 mV/group) is obtained for the Fe(III)/Fe(II) reactions of compounds **10**, **16**, and **20**. This linear free energy relationship is shown in Figure 5 and is identical to that reported for three Cu(III) corroles having almost the same structures as compounds **9**, **15**, and **19**.[32]

Figure 5, which compares substituent effects for the Fe(III) and Cu(III) corroles containing NO_2 substituents at the **3** and **17** positions of the macrocycle, also includes data on a series of Ge(IV) corroles,[33] which are structurally similar to the Group A compounds in Chart 1. For this series of compounds, only macrocycle-centered reactions occur, and the first reduction and first oxidation generate the Ge(IV) corrole π-anion and π-cation radicals, respectively. For the compounds in Chart 1, the ~200 mV shift in $E_{1/2}$ per each nitro group at the 3 and 17 positions of the macrocycle is larger than the 70−80 mV shift in $E_{1/2}$ for each nitro group at the *meso*-phenyl position of the triarylcorroles. This difference in substituent effect can best be seen by comparisons of the $Fe^{III/II}$ reduction potentials for **9** and **10** ($\Delta E_{1/2}$ = 0.21 V), **15** and **16** ($\Delta E_{1/2}$ = 0.21 V), and **19** and **20** ($\Delta E_{1/2}$ = 0.23 V). This decreased substituent effect for *meso*-phenyl substituents is as expected and consistent with data in the literature for other porphyrins, corroles, and related macrocycles.[29,30,32,34−37] In summary, the largest substituent effect occurs for NO_2 groups at the β-pyrrole positions of the corrole macrocycle and the smallest for NO_2 substituents at the *para*-phenyl groups of the triarylcorrole.

In contrast to what is seen for the Group A compounds, the redox behavior of the Group B compounds differs substantially. This is because the electrode reactions of **10**, **16**, and **20** involve not only the central metal ion and conjugated macrocycle but also the electroactive $C_6H_4NO_2$ group[38] on each *meso*-position of the triarylcorrole. The reduction of nitrobenzene in CH_2Cl_2 is located at $E_{1/2}$ = −1.08 V,[31] and exactly the same half-wave potential is seen for reduction of the *meso*-$C_6H_4NO_2$ groups on (TNPC)FeNO **10** where the current is approximately three times that of the preceding Fe(III)/Fe(II) reaction (see

dx.doi.org/10.1021/ic3002459 | *Inorg. Chem.* 2012, 51, 3910−3920

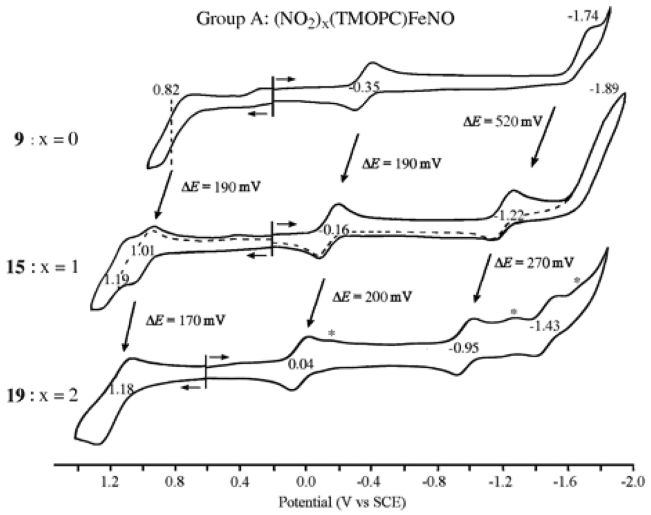

Figure 3. Cyclic voltammograms of (TMOPC)FeNO **9**, 3-NO_2-(TMOPC)FeNO **15**, and 3,17-$(NO_2)_2$-(TMOPC)FeNO **19** in CH_2Cl_2 containing 0.1 M TBAP. The reduction peaks of **19** marked by asterisks are mostly likely due to Fe species with an unknown sixth axial ligand.

voltammogram in Figure 4a). This result is consistent with a one electron addition in the first step and three overlapping one-electron transfers in the second where the overall reduction

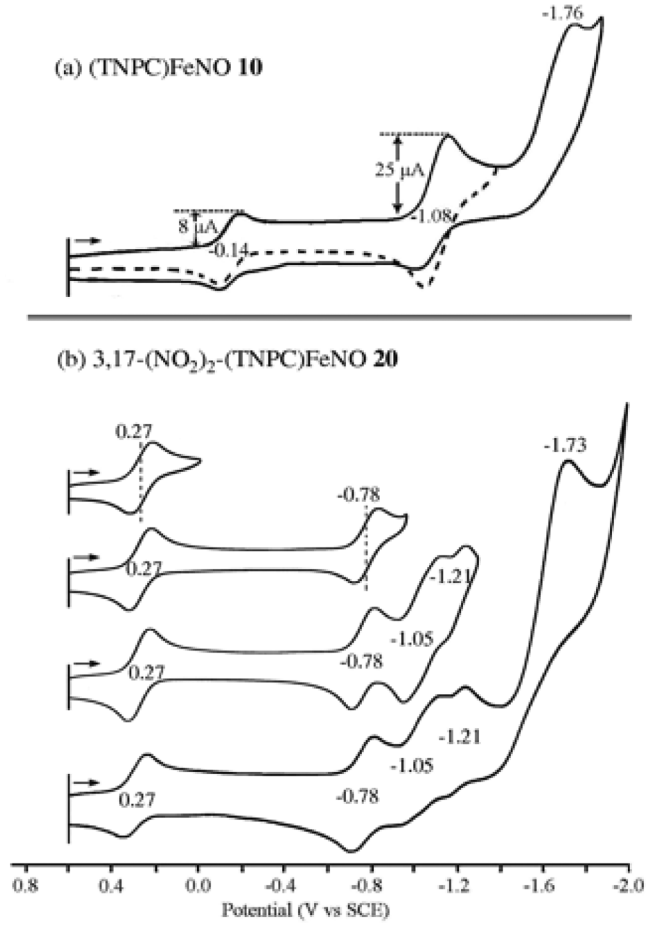

Figure 4. Cyclic voltammograms of (TNPC)FeNO **10** and 3,17-$(NO_2)_2$-(TNPC)FeNO **20** in CH_2Cl_2 containing 0.1 M TBAP.

processes can be described as shown by eqs 1 and 2. A single multielectron reduction of *meso*-$C_6H_4NO_2$ groups has previously been reported for copper triarylcorroles[39] as well as for tetraphenylporphyrins having the same electroactive substituents at the four *meso*-positions of the macrocycle.[34,35]

$$(\mathrm{TNPC})\mathrm{Fe^{III}(NO)} + \mathrm{e} \rightleftharpoons [(\mathrm{TNPC})\mathrm{Fe^{II}(NO)}]^- \quad E_{1/2} = -0.14\ \mathrm{V} \tag{1}$$

$$[(\mathrm{TNPC})\mathrm{Fe^{II}(NO)}]^- + 3\mathrm{e} \rightleftharpoons [(\mathrm{TNPC})\mathrm{Fe^{II}})(\mathrm{NO})]^{4-} \quad E_{1/2} = -1.08\ \mathrm{V} \tag{2}$$

The fact that only a single reduction peak is seen for the overall three electron conversion of $[(\mathrm{TNPC})\mathrm{Fe^{II}(NO)}]^-$ to $[(\mathrm{TNPC})\mathrm{Fe^{II}})(\mathrm{NO})]^{4-}$ (eq 2) is consistent with a lack of any interaction between the three *meso*-$C_6H_4NO_2$ groups of the corrole, each of which is reduced by one electron at the same potential of $E_{1/2} = -1.08$ V vs SCE. This is not the case for **16** and **20** where the three one-electron reductions of $C_6H_4NO_2$ each occur at separate half wave potentials as illustrated in Figure 4b for the case of 3,17-$(NO_2)_2$-(TNPC)FeNO **20**. For this compound, three reversible one electron reductions are seen at $E_{1/2} = -0.78$, -1.05, and -1.21 V and the first four reductions can be described by eqs 3–6.

$$(\mathrm{NO_2})_2(\mathrm{TNPC})\mathrm{Fe^{III}(NO)} + \mathrm{e} \rightleftharpoons [(\mathrm{NO_2})_2(\mathrm{TNPC})\mathrm{Fe^{II}(NO)}]^- \quad E_{1/2} = 0.27\ \mathrm{V} \tag{3}$$

$$[(\mathrm{NO_2})_2(\mathrm{TNPC})\mathrm{Fe^{II}(NO)}]^- + \mathrm{e} \rightleftharpoons [(\mathrm{NO_2})_2(\mathrm{TNPC})\mathrm{Fe^{II}})(\mathrm{NO})]^{2-} \quad E_{1/2} = -0.78\ \mathrm{V} \tag{4}$$

$$[(\mathrm{NO_2})_2(\mathrm{TNPC})\mathrm{Fe^{II}(NO)}]^{2-} + \mathrm{e} \rightleftharpoons [(\mathrm{NO_2})_2(\mathrm{TNPC})\mathrm{Fe^{II}})(\mathrm{NO})]^{3-} \quad E_{1/2} = -1.05\ \mathrm{V} \tag{5}$$

$$[(\mathrm{NO_2})_2(\mathrm{TNPC})\mathrm{Fe^{II}(NO)}]^{3-} + \mathrm{e} \rightleftharpoons [(\mathrm{NO_2})_2(\mathrm{TNPC})\mathrm{Fe^{II}})(\mathrm{NO})]^{4-} \quad E_{1/2} = -1.21\ \mathrm{V} \tag{6}$$

The site of the electron transfer for each redox reaction can be assigned on the basis of thin-layer UV–vis and FT-IR spectroelectrochemistry. For example, the first oxidation of **15** involves an Fe^{III}/Fe^{III} π-cation radical process as confirmed by thin-layer UV–vis spectroelectrochemistry. As shown in Figure 6a, the controlled potential reduction of **15** at 1.10 V in CH_2Cl_2 results in a loss of the Soret band intensity at 431 nm and the appearance of absorptions between 600 and 900 nm, which are characteristic of a corrole π-cation radical. Shifting the applied potential from 1.10 to 1.25 V then leads to a species, the UV–visible spectrum of which has a broad band at 650–900 nm and a weak band in the Soret region at 380 nm (see Figure 6b). Electrogenerated Fe^{IV} corroles have been characterized by a Soret band at 372–381 nm,[40] and the second oxidation of **15** is assigned as a metal-centered process to give an Fe^{IV} π-corrole radical.

dx.doi.org/10.1021/ic3002459 | Inorg. Chem. 2012, 51, 3910–3920

Table 2. Half-Wave or Peak Potentials (V vs. SCE) of Investigated Ion Corroles in CH_2Cl_2, 0.1 M TBAP

		oxidation		reduction				
	compound no.	2nd	1st	metal (Fe^{3+}/Fe^{2+})	macrocycle			
group A	**9**	0.82[a]	0.82[a]	−0.35		−1.74[b]		
	15	1.19	1.01	−0.16		−1.22	−1.89[b]	
	19	1.18[a]	1.18[a]	0.04		−0.95	−1.43	
group B	**10**	1.18[b]	0.97	−0.14		−1.08[a]	−1.76[b]	
	16	1.48[b]	1.18	0.05		−1.05	−1.38	
	20	1.46[b]	1.32	0.27	−0.78	−1.05	−1.21	−1.73
$C_6H_5NO_2$						−1.08[c]		

[a]Overlapping. [b]Peak potential at a scan rate of 0.1 V/s. [c]Data taken from ref 31.

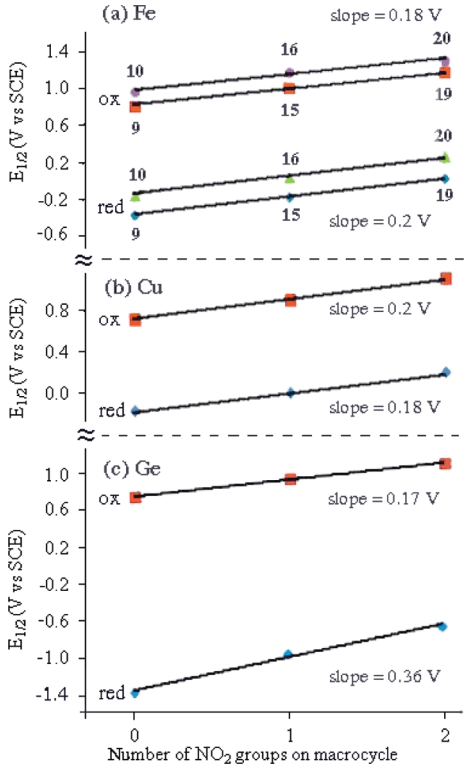

Figure 5. Correlation between the number of nitro groups on the corrole macrocycle and $E_{1/2}$ for the first reduction and the first oxidation in CH_2Cl_2, 0.1 M TBAP of (a) $(NO_2)_x$TNPCFe^{III}NO (**10**, **16**, and **20**) and $(NO_2)_x$TMOPCFe^{III}NO (**9**, **15**, and **19**), (b) $(NO_2)_x$TtBuPCorrCu^{III}, and (c) $(NO_2)_x$TPCorrGe^{IV}(OCH_3). Data for the Cu(III) and Ge(IV) compounds were taken form refs 32 and 33.

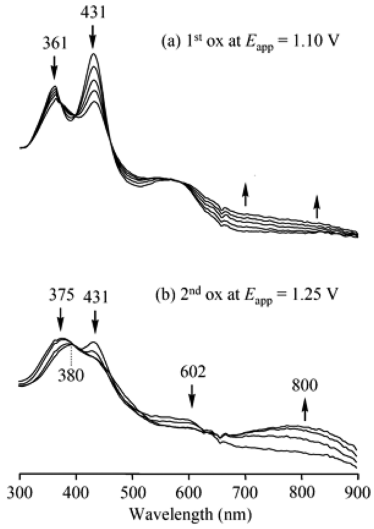

Figure 6. Thin-layer UV−vis spectral changes of **15** during the first and the second oxidation in CH_2Cl_2, 0.2 M TBAP.

UV−visible spectral changes monitored during the first one-electron reduction of the six corroles in Chart 1 are illustrated in Figure 7. A previous spectroelectrochemical study of Cu(III) corroles with Group A type structures showed the presence of quite distinctive absorption bands for the singly reduced, formally Cu(II), forms of the compound containing one or two NO_2 substituents on the macrocycle, and this is also the case for the four examined iron-nitrosyl corroles bearing the same substitution pattern (**15**, **16**, **19**, and **20**).

The UV−visible spectra of the neutral corroles in Group A all possess a split Soret band at 366−431 nm and a weak intensity visible band at 531−591 nm. The Soret band is located at 366 and 416 nm for **9**, at 359 and 431 nm for **15**, and at 347 and 423 nm for **19**. This contrasts with spectra for the neutral Group B corroles, which have a single Soret band at 383 to 403 nm and one or two visible bands at 540−611 nm (see Figure S3, Supporting Information, and Figure 7).

A comparison of spectra for the singly reduced iron nitrosyl corroles in CH_2Cl_2 (Figure 7) with those of related singly reduced Cu(III) corroles in PhCN (Figure 5 in ref 32) shows almost the same evolution of spectral shape upon going from the corroles with no nitro substituents at the β-pyrrole position (compounds **9** and **10**) to derivatives with one or two NO_2 groups at the 3 or 3,17 positions of the macrocycle (compounds **15**, **16**, **19**, and **20**). The spectrum of singly reduced **9** and **10** suggests formation of an Fe(II) nitrosyl corrole product, and this assignment may also be true for the other four compounds, each of which possess two strong absorptions between 600 and 750 nm.

It should be noted that the spectrum of singly reduced **15** has bands at 475, 618, and 728 nm as compared to 463, 637, and 714 nm for singly reduced **16**, with both species lacking a major absorption in the Soret region of the spectrum. A similar spectral shape is also seen for singly reduced **19** and **20**. Compound **19**, after reduction, has bands at 490, 630, and 740 nm, as compared to singly reduced **20**, which has bands at 483, 652, and 722 nm. Again, the overall shapes of the UV−visible spectra are quite similar to those for singly reduced Cu(III) corroles having nitro groups at the same β-pyrrole positions of corrole macrocycle.

To further investigate the site of electron transfer, FT-IR spectroelectrochemistry was used to monitor the NO stretching vibrational bands during the first reduction of compounds **15**

dx.doi.org/10.1021/ic3002459 | Inorg. Chem. 2012, 51, 3910−3920

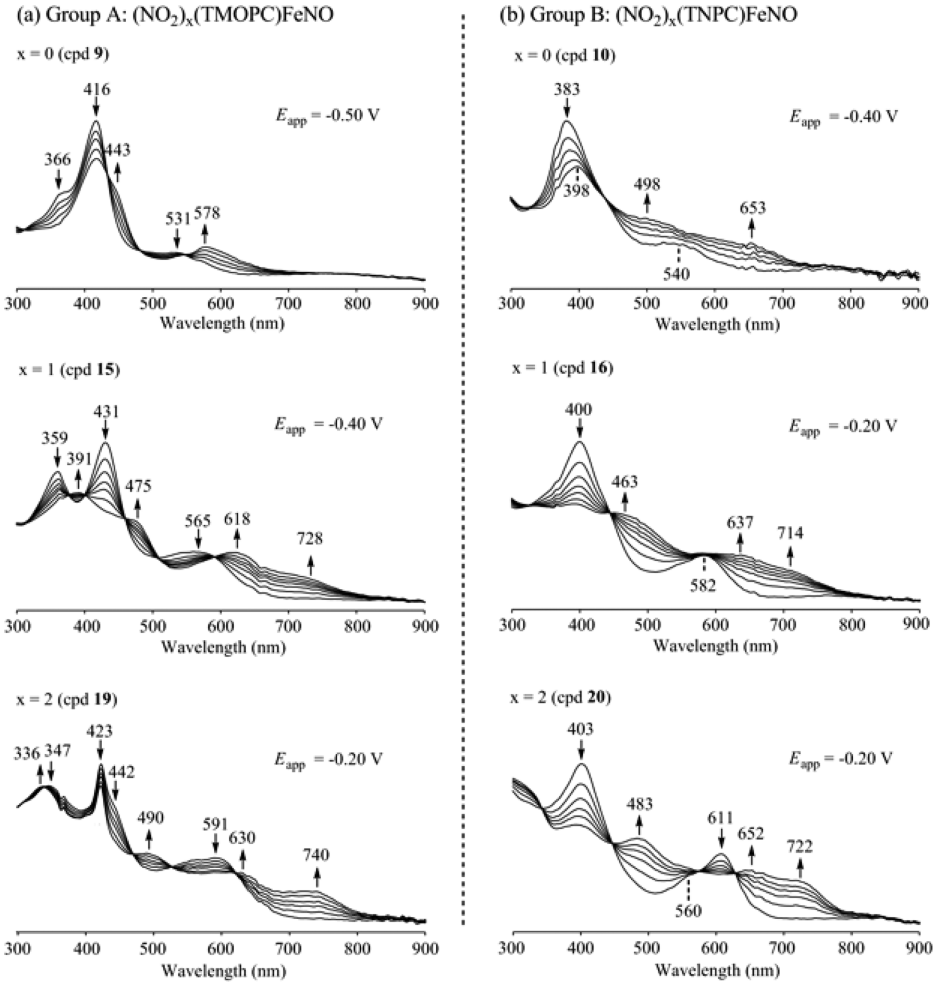

Figure 7. UV−visible changes recorded during the first reduction of (a) $(NO_2)_x$(TMOPC)FeNO (Goup A) and (b) $(NO_2)_x$(TNPC)FeNO (Group B) in CH_2Cl_2, 0.1 M TBAP.

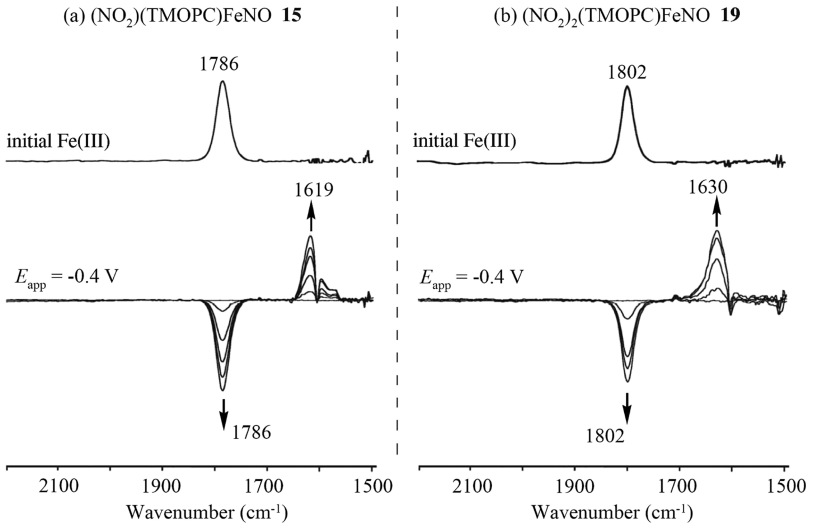

Figure 8. Thin-layer IR spectral changes during the first one-electron reduction of (a) **15** and (b) **19** in CH_2Cl_2, 0.1 M TBAP upon the indicated potentials.

and **19** in CH_2Cl_2. The relevant spectroelectrochemical data are shown in Figure 8 before and after reduction at an applied potential of −0.4 V. As seen in the Figure, the neutral corroles exhibit well-defined NO bands at 1786 (**15**) cm^{-1} and 1802 (**19**), while the singly reduced forms of the compounds have bands at 1619 (**15**) and 1630 (**19**) cm^{-1}. The latter is consistent with what has been reported for other Fe^{II} corroles that exhibit a NO band at 1585−1760 cm^{-1}.[41]

dx.doi.org/10.1021/ic3002459 | *Inorg. Chem.* 2012, 51, 3910−3920

Attempts to determine the NO stretching frequencies of the singly oxidized corroles were less successful due to the rapid loss of NO, which occurs after conversion to the Fe(IV) form of the compounds. When an oxidizing potential of 1.1 V was applied to a solution of **15**, a new weak transient band appeared at 1813 nm^{-1}, consistent with the initial formation of an Fe(III) corrole π-cation radical,[41] but when an oxidizing potential of 1.25 V was applied to the solution, the 1813 cm^{-1} band disappeared, indicating complete loss of the nitrosyl axial ligand during the second oxidation of **15**. Compound **19** undergoes an overlapping two electron abstraction in the first oxidation (see Figure 3), and the NO seems to be lost during this process.

CONCLUSIONS

We report here an efficient synthetic protocol for the preparation of β-nitro substituted iron corroles, obtained by reaction of the starting triarylcorrole iron chloride complex with $NaNO_2$ in DMF. By tuning the reaction conditions, it is possible to obtain both the 3-nitro and the 3,17-dinitro derivatives in satisfying yields. The scope of the reaction is quite general, and nitro substituted iron corroles can be obtained with a wide range of triarylcorroles, although in some cases the corresponding μ-oxo dimer, instead the nitrosyl iron complex, is obtained as the reaction side product. The π-cation radical nature of the iron corrole complex can be confidently assigned considering the reactive species, which undergoes nucleophilic attack by nitrite ion, leading to the β-nitro functionalized product.

A detailed study of electrochemistry and spectroelectrochemistry of β-nitro substituted iron corroles is also presented, elucidating the site of electron transfer and the influence of the peripheral nitro groups. The results obtained provide novel insights on these species, showing that the effect of the nitro substituents on the redox behavior is similar to what is observed for analogous copper(III) corroles having the same substitution pattern.

ASSOCIATED CONTENT

Supporting Information

Crystal data and views of the molecular structure of **17** and the corresponding CIF file and UV−visible spectra of $(NO_2)_x$(TMOPC)FeNO and $(NO_2)_x$(TNPC)FeNO. This material is available free of charge via the Internet at http://pubs.acs.org.

AUTHOR INFORMATION

Corresponding Author

*E-mail: kkadish@uh.edu (K.M.K.), kmsmith@lsu.edu (K.M.S.), roberto.paolesse@uniroma2.it (R.P.).

Notes

The authors declare no competing financial interest.

ACKNOWLEDGMENTS

The authors thank the Italian MIUR (R.P., PRIN2009 Project 2009Z9ASCA_004), US National Institutes of Health (K.M.S., Grant CA132861), and the Robert A. Welch Foundation (K.M.K., Grant E-680).

REFERENCES

(1) Johnson, A. W.; Kay, I. T. *J. Chem. Soc.* **1965**, 1620.
(2) (a) Gross, Z.; Aviv-Harel, I. *Chem.—Eur. J.* **2009**, *15*, 8382−8394. (b) Kupershmidt, L.; Okun, Z.; Amit, T.; Mandel, S.; Saltsman, I.; Mahammed, A.; Bar-Am, O.; Gross, Z.; Youdim, M. B. H. *J. Neurochem.* **2010**, *113*, 363−373. (c) Kanamori, A.; Catrinescu, M. M.; Mahammed, A.; Gross, Z.; Levin, L. A. *J. Neurochem.* **2010**, *114*, 488−498.
(3) (a) Barbe, J.-M.; Canard, G.; Brandès, S.; Guilard, R. *Chem.—Eur. J.* **2007**, *13*, 2118. (b) He, C.-L.; Ren, F. L.; Zhang, X.-B.; Han, Z.-X. *Talanta* **2006**, *70*, 364. (c) Gatto, E.; Malik, M. A.; Di Natale, C.; Paolesse, R.; D'Amico, A.; Lundström, I; Filippini, D. *Chem.—Eur. J.* **2008**, *14*, 6057. (d) Paolesse, R.; Mandoj, F.; Marini, A.; Di Natale, C. In *Encyclopedia of Nanoscience and Nanotechnology*; Nalwa, H., Ed.; American Science Publishers: Valencia, CA, 2004. (e) Andrioletti, B.; Rose, E. *J. Chem. Soc., Perkin Trans. 1* **2002**, 715−716.
(4) Paolesse, R. *Synlett* **2008**, 2215.
(5) Gryko, D. T.; Fox, J. P.; Goldberg, D. P. *J. Porphyrins Phthalocyanines* **2004**, *8*, 1091.
(6) Nardis, S.; Monti, D.; Paolesse, R. *Mini-Rev. Org. Chem.* **2005**, *2*, 546.
(7) Lemon, C. M.; Brothers, P. J. *J. Porphyrins Phthalocyanines* **2011**, *42*, 39.
(8) Gross, Z.; Aviv-Harel, I. *Coord. Chem. Rev.* **2011**, *255*, 717−736.
(9) Saltsman, I.; Mahammed, A.; Goldberg, I.; Tkachenko, E.; Botoshansky, M.; Gross, Z. *J. Am. Chem. Soc.* **2002**, *124*, 7411−7420.
(10) Ghosh, A.; Wondimagegn, T.; Parusel, A. B. J. *J. Am. Chem. Soc.* **2000**, *122*, 5100.
(11) Walker, F. A.; Licoccia, S.; Paolesse, R. *J. Inorg. Biochem.* **2006**, *100*, 810 and references therein.
(12) Stefanelli, M.; Nardis, S.; Tortora, L.; Fronczek, F. R.; Smith, K. M.; Licoccia, S.; Paolesse, R. *Chem. Commun.* **2011**, *47*, 4255−4257.
(13) Ye, S.; Tuttle, T.; Bill, E.; Simkhovich, L.; Gross, Z.; Thiel, W.; Neese, F. *Chem.—Eur. J.* **2008**, *14*, 10839.
(14) Kadish, K. M.; Mu, X. H.; Lin, X. Q. *Electroanalysis* **1989**, *1*, 35−41.
(15) Paolesse, R. In *The Porphyrin Handbook*; Kadish, K. M., Smith, K. M., Guilard, R., Eds.; Academic Press: New York, 2000; Vol. *2*, pp 201−232.
(16) Gryko, D. T. *J. Porphyrins Phthalocyanines* **2008**, *12*, 906.
(17) Gross, Z.; Galili, N.; Saltsman, I. *Angew. Chem., Int. Ed.* **1999**, *38*, 1427−1429.
(18) Joseph, C. A.; Lee, M. S.; Iretskii, A. V.; Wu, G.; Ford, P. C. *Inorg. Chem.* **2006**, *45*, 2075−2082.
(19) Simkhovich, L.; Goldberg, I.; Gross, Z. *Inorg. Chem.* **2002**, *41*, 5433−5439.
(20) Altomare, A.; Burla, M. C.; Camalli, M.; Cascarano, G. L.; Giacovazzo, C.; Guagliardi, A.; Moliterni, A. G. G.; Polidori, G.; Spagna, R. *J. Appl. Crystallogr.* **1999**, *32*, 115−119.
(21) Sheldrick, G. M. *Acta Crystallogr., Sect. A* **2008**, *64*, 112−122.
(22) Spek, A. L. *J. Appl. Crystallogr.* **2003**, *36*, 7−13.
(23) Wehman, P; Borst, L; Kamer, P. C. J.; van Leeuwen, P. W. N. M. *J. Mol. Catal. A* **1996**, *112*, 23−26.
(24) Simkhovich, L.; Mahammed, A.; Goldberg, I.; Gross, Z. *Chem.—Eur. J.* **2001**, *7*, 1041−1055.
(25) Autret, M.; Will, S.; van Caemelbecke, E.; Lex, J.; Gisselbrecht, J.-P.; Gross, M.; Vogel, E.; Kadish, K. M. *J. Am. Chem. Soc.* **1994**, *116*, 9141−9149.
(26) Bröring, M.; Milsmann, C.; Ruck, S.; Köhler, S. *J. Organomet. Chem.* **2009**, *694*, 1011−1015.
(27) Simkhovich, L.; Galili, N.; Saltsman, I.; Goldberg, I.; Gross, Z. *Inorg. Chem.* **2000**, *39*, 2704−2705.
(28) Nardis, S.; Paolesse, R.; Licoccia, S.; Fronczek, F. R.; Vicente, M. G. H.; Shokhireva, T. K.; Cai, S.; Walker, F. A. *Inorg. Chem.* **2005**, *44*, 7030−7046.
(29) Kadish, K. M.; Van Caemelbecke, E.; Royal, G. In *The Porphyrin Handbook*; Kadish, K. M., Smith, K. M., Guilard, R., Eds.; Academic Press: San Diego, CA, 2000; Vol. *8*, pp 1−97.
(30) Kadish, K. M.; Royal, G.; Caemelbecke, V. E.; Gueletti, E. In *The Porphyrin Handbook*; Kadish, K. M., Smith, K. M., Guilard, R., Eds.; Academic Press: San Diego, CA, 2000; Vol. *9*, pp 1−419.

(31) Kadish, K. M.; E, W.; Sintic, P. J.; Ou, Z.; Shao, J.; Ohkubo, K.; Fukuzumi, S.; Govenlock, L. J.; McDonald, J. A.; Try, A. C.; Cai, Z.-L.; Reimers, J. R.; Crossley, M. J. *J. Phys. Chem. B* **2007**, *111*, 8762−8774.
(32) Stefanelli, M.; Mandoj, F.; Mastroianni, M.; Nardis, S.; Mohite, P.; Fronczek, F. R.; Smith, K. M.; Kadish, K. M.; Xiao, X.; Ou, Z.; Chen, P.; Paolesse, R. *Inorg. Chem.* **2011**, *50*, 8281−8292.
(33) Mastroianni, M.; Zhu, W.; Stefanelli, M.; Nardis, S.; Fronczek, F. R.; Smith, K. M.; Ou, Z.; Kadish, K. M.; Paolesse, R. *Inorg. Chem.* **2008**, *47*, 11680−11687.
(34) Ghosh, A.; Halvorsen, I.; Nilsen, H. J.; Steene, E.; Wondimagegn, T.; Lie, R.; Van Caemelbecke, E.; Gou, N.; Ou, Z.; Kadish, K. M. *J. Phys. Chem. B* **2001**, *105*, 8120−8124.
(35) Schiavon, M. A.; Iwamoto, L. S.; Ferreira, A. G.; Iamamoto, Y.; Zanoni, M. V. B.; Assis, M. D. *J. Braz. Chem. Soc.* **2000**, *11*, 458−466.
(36) Bachmann, J.; Nocera, D. G. *J. Am. Chem. Soc.* **2005**, *127*, 4730−4743.
(37) Ozette, K.; Battioni, P.; Leduc, P.; Bartoli, J-F; Mansuy, D. *Inorg. Chim. Acta* **1998**, *272*, 4−6.
(38) Lund, H. Organic Electrochemistry. In *Cathodic reduction of nitro and related compounds*, 4th ed.; Lund, H., Hammerich, O., Eds.; Marcel Dekker, Inc.: New York, 2001; pp 379−409.
(39) Bhattacharya, D.; Singh, P.; Sarkar, S. *Inorg. Chim. Acta* **2010**, *363*, 4313−4318.
(40) Van Caemelbecke, E.; Will, S.; Autret, M.; Adamian, V. A.; Lex, J.; Gisselbrecht, J.-P.; Gross, M.; Vogel, E.; Kadish, K. M. *Inorg. Chem.* **1996**, *35*, 184−192.
(41) Autret, M.; Will, S.; Van Caemelbecke, E.; Lex, J.; Gisselbrecht, J. P.; Gross, M.; Vogel, E.; Kadish, K. M. *J. Am. Chem. Soc.* **1994**, *116*, 9141−9149.